Hierarchical Characterization of Aggregates for Monte Carlo Simulations

Heiko Briesen
Lehrstuhl für Prozesstechnik, RWTH Aachen University, Turmstraße 46, D-52056 Aachen, Germany

DOI 10.1002/aic.10881
Published online April 26, 2006 in Wiley InterScience (www.interscience.wiley.com).

Modeling of crystallization processes is usually based on deterministic population balances. Although conceptually there is no such limitation, population balance modeling is used only up to a few internal dimensions because of the computational effort. Alternatively, Monte Carlo methods are increasingly used for the simulation of particulate systems. There, the characterization of particles is also often limited to a few size and shape parameters similar to those of deterministic population balance modeling. A major advantage of Monte Carlo methods, however, is its simple extensibility to more complex particle characterizations. However, actually considering the full three-dimensional shape of a complex agglomerate may lead to a prohibitive computational effort. To overcome this bottleneck a hierarchical particle characterization is proposed. This characterization allows the realistic representation of the agglomerates, without the need for detailed geometric computations for each particle. Instead of the full geometry, substitution systems are introduced that can be used to perform aggregation events or to identify crystal faces that are available for growth. The substitution systems consist of point mass systems, which preserve certain characteristics of the original agglomerate such as the moment of inertia. Numerical studies show the applicability of the approach. Based on this characterization, modeling of rate processes can be performed on a much higher level of detail than is allowed by standard one- or two-dimensional particle characterizations. © 2006 American Institute of Chemical Engineers *AIChE J,* 52: 2436–2446, 2006

Keywords: Monte Carlo, stochastic modeling, population balance, crystallization, aggregation, agglomeration, agglomerate structure

Introduction

Modeling of disperse-phase processes is often based on the population balance equation (PBE). It allows evaluation of the deterministic evolution of particle size distribution. Introduced by Hulburt and Katz,[1] population balances have gained ever-increasing popularity for the modeling of various applications dealing with dispersed-phase systems (crystallization, cloud droplet formation, aerosol reactors, polymerization, etc.). In particular, crystallization is a main application for population balance modeling probably induced by the pioneering textbook by Randolph and Larson,[2] which strongly focuses on this topic. Over the past decades numerous solution techniques for the PBE have been developed and successfully applied to a variety of problems (see work by Kumar and Ramkrishna[3-5] and references therein). However, most of these techniques deal with the solution of population balance models with only one internal dimension. A one-dimensional approach may, for example, be reasonably applicable to droplets in emulsions, which usually form spheres. Also in crystallization mostly a one-dimensional characterization of crystal size has been used. Depending on the objective of the simulation, a characteristic crystal length (length, width, volume equivalent sphere diameter, etc.) or the particle volume may be chosen.

Correspondence concerning this article should be addressed to H. Briesen at briesen@lfpt.rwth-aachen.

On the other hand, it is well known that real crystals can hardly ever be represented by one characteristic length. Even nonagglomerated crystalline particles can exhibit complex shapes[6] that can strongly affect the value of the product. Especially for high added-value products such as pharmaceuticals, the shape—besides the polymorphic form—is of major interest. Disregarding any population of particles, a general problem is to predict the stationary complex shape of growing crystals. Modern approaches to its solution try to correlate the growth rate of the several crystal faces to the attachment energy of single molecules to the crystalline structure. Reviews on this topic have been given by Winn and Doherty[7] and Bennema et al.[8]

Considering agglomerated crystals, a detailed characterization is even more difficult. To fully characterize a particle with a complex habit of the primary crystals and an agglomerate structure, many inner variables are needed. Modeling a process on the basis of such a detailed characterization by means of a population balance approach would consequently lead to a high-dimensional partial differential equation, which poses considerable challenges on solution techniques.

Although primary particle shape and agglomerate structure affect downstream processing properties such as filterability, flowability, or mechanical stability, the detailed crystal shape is rarely considered. Also the rate processes determining the crystallization behavior depend on the shape properties of the particles.[9] This deficiency is probably one of the reasons that crystallization models for industrial processes have not yet reached the same level of predictiveness as models for standard fluid-phase processes such as distillation.

To overcome this deficiency a number of researches have worked on developing models and solution techniques for higher-dimensional PBEs. In fact, Hulburt and Katz[1] themselves formulated the population balance with an arbitrary number of internal coordinates and derived solution techniques on the basis of the method of moments for the one- and two-dimensional cases. More recently, some researchers investigated the simultaneous evolution of particles size and shape[10-13] using a characterization in which both the length and width of crystals are considered. Zhang and Doherty[14] coupled a separate shape evolution model[15] with a standard one-dimensional population balance model, which also allowed simultaneous tracking of particle size and shape.

Fractal aggregate structures are also frequently investigated in the context of aerosol processes. There, the structure of aggregates is predicted by cluster–cluster aggregation algorithms based on pioneering work by Witten and Sander[16] or by cluster evolution[17] arising from coagulation and sintering. However, contrary to this study, parallel crystal surface growth, which is essential for crystallization, is to the author's knowledge usually not considered. Also these studies are mostly limited to one or a low number of clusters and use simple geometries (spheres) for characterization of the primary particles.

Besides for the modeling of complex shape, two-dimensional particle characterizations have also been used to address other crystallization problems as well as applications different from crystallization. Induced by the discussion on the effect of inner lattice strain on the growth of crystals,[18] Gerstlauer et al.[19] formulated a two-dimensional population balance model considering particle size and inner strain as two independent inner coordinates and solved the model by means of a nonequidistant finite-volume method.

Despite the progress achieved for multidimensional population balance modeling, several authors[20-23] state that the use of deterministic techniques to solve the PBE will face restrictions because of the complexity of implementation and the computational load when further increasing the dimension of particle characterization. Instead, they all explore stochastic (or so-called Monte Carlo) techniques to solve population balance problems. Monte Carlo techniques explicitly monitor the evolution of an ensemble of discrete particles by artificially realizing probabilistically selected events. Because the different methods are developed for different fields of application, only the methodological characteristics of the methods will be briefly reviewed, irrespective of the actual technical problem.

Monte Carlo solution techniques were first introduced by Metropolis and Ulam.[24] Although they addressed several problems in physics, Spielman and Levenspiel[25] were the first to use the Monte Carlo approach to solve problems involving dispersed-phase systems by investigating the behavior of a two-phase reactor. Especially for a small number of particles where the continuity assumptions of the PBE are inherently violated, stochastic methods can be used.[26] Later on the theoretical connection between the deterministic PBE and stochastic solution methods were established by Ramkrishna,[27] basically showing their equivalency.

Current Monte Carlo methods for solving population balance problems may be categorized by means of the selection of the time step. In time-driven Monte Carlo simulations a time interval is chosen and the algorithm performs a number of events that probabilistically occur during this interval.[20,28] Thus, the time steps have to be chosen explicitly by the user or an appropriate algorithm. During this time step several events are performed on the basis of the rate expressions. In case of an event-driven Monte Carlo simulation[21,29,30] an interevent time is computed on the basis of the active rate expressions. After this time step one of the possible events is probabilistically selected.

Another distinguishing property of Monte Carlo methods for population balance problems is the choice of the control volume. Obviously, the number of particles in the actual physical system (such as the crystallization vessel) is far too large to be used for simulation purposes. Instead a small control volume is chosen that consists of a representative sample of the particle population. This control volume can be chosen to be fixed.[20,26] If the number of particles within this control volume is about to change (which is the case for all rate processes apart from growth), this affects the statistical significance of the sample. To remedy this, the control volume can be adapted over the simulation time on the basis of certain criteria (such as whether the particle number has halved[21,31]) or after each step to ensure a constant number of particles.[23,29]

Monte Carlo techniques can of course also be used for the simulation of one-dimensional population balance problems,[29,32] although the benefit compared against deterministic methods is questionable.[22] Generally, a number of studies have shown the benefit of Monte Carlo methods for the simulation of multidimensional population balance problems.[20,22,30,33] Only the work by van Peborgh Gooch and Hounslow[20] explicitly deals with crystallization. In their most complex example they used a four-dimensional crystal characterization using size,

growth rate, number of primary crystals in an agglomerate, and the number of slow growing primary crystals in an agglomerate as internal coordinates.

Monte Carlo methods are distinct for their simplicity in implementation and the flexibility to incorporate the underlying physics in the model. Incorporating more complex physics in the model on the other side increases the computational effort. For multidimensional problems, for example, an increasing number of discrete particles is needed to ensure statistically relevant results. However, these complex problems are hardly accessible by deterministic approaches in the first place. Furthermore, the computational load will only limit the efficiency but not the general applicability to complex problems. With the expected gain in computational power, the range of manageable problems will continuously increase.

A further disadvantage of Monte Carlo methods is that model-based techniques (optimization, parameter estimation, model-based control) usually used with deterministic models may be more difficult to realize. However, attempts to carry over the methodologies from equation-based models have already been made.[34]

To the author's knowledge, there is no study that actually addresses the evolution of a particle population in which the particles are characterized reflecting a realistic geometric shape. Because of the difficulty to experimentally investigate complex shaped particles, this may not seem to be a major drawback. However, recent advances in measurement technology based on image analysis[35-37] are about to overcome this experimental deficiency.

From a modeling perspective, a fully detailed characterization indeed seems infeasible, given that a huge number of internal coordinates would be needed as a result of the huge number of geometrical degrees of freedom. Thus, there is a need for a reduced characterization that is still capable of reflecting a realistic geometric shape.

In the present contribution a hierarchical particle characterization will be presented, in which the geometric complexity is represented on different levels of detail. This is done by introducing a substitute particle characterization instead of the full detailed characterization. Because of the complexity of the presented example, the PBE itself will not even be considered. Instead the model will be formulated directly in the sense of the Monte Carlo approach. The focus of this contribution will be on the methodological development. For the considered rate processes (growth and agglomeration), simple expressions are used that do not reflect the actual rates of a specific crystalline substance or a specific experimental configuration.

Methodology

Hierarchical particle characterization

Primary Particle Characterization. Most of the crystals that appear in industrial processes exhibit a needle- or plate-like habit. The characterization of the primary particles, therefore, has to be able to reflect this observation. The primary particles are modeled as arbitrary cuboids for which three independent side length halves l_1, l_2, and l_3 must be specified (see Figure 1). The complexity of this system can be reduced by assuming that two of the side lengths are equal, which would still allow characterization of needle- and plate-like habits. Also a characterization of the primary particles as spheres, which might be appropriate for aerosol processes, would simplify the characterization. Obviously, additional complex shapes may also be considered. For the full shape characterization of arbitrary crystals, many more than three characterizing lengths may possibly be necessary. The chosen characterization using three independent side length halves, however, is already capable of reflecting the main geometric properties of many primary particles.

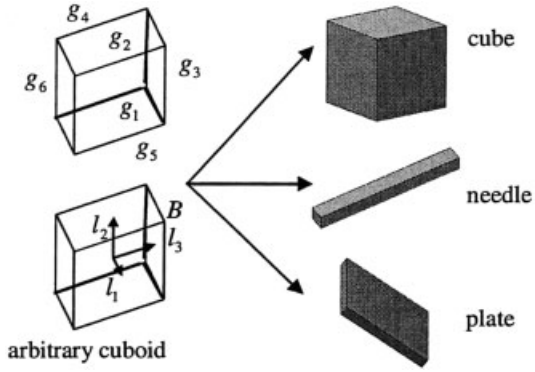

Figure 1. Primary particle characterization as an arbitrary cuboid.

Agglomerate Characterization. Agglomerates consist of a number of primary particles with a relative position to each other. To determine this relative position, two coordinate systems are introduced: the coordinate system of a primary particle object and the coordinate system of an agglomerate object. If the relative position of different agglomerates would be of interest, one could additionally construct a third coordinate system reflecting the actual three-dimensional space.

Each of the primary particles has its own coordinate system. The origins of these coordinate systems are the center of mass of the respective primary particle. The orientation is given such that the axis x_1, x_2, and x_3 are parallel to the side length halves l_1, l_2, and l_3, respectively. The coordinate system for one primary particle is also depicted in Figure 1. Consequently, the corner B in Figure 1 can be expressed in homogeneous coordinates by $\boldsymbol{x}_B = (l_1, l_2, l_3, 1)^T$. The concept of homogeneous coordinates is borrowed from computer graphics.[38] It enables one to code arbitrary affine mappings as one single matrix operation. Considering a general affine mapping in three-dimensional Cartesian coordinates [index (c)]

$$\boldsymbol{x}'_{(c)} = \boldsymbol{A}\boldsymbol{x}_{(c)} + \boldsymbol{t} \qquad \text{with } \boldsymbol{x}'_{(c)}, \boldsymbol{x}_{(c)}, \boldsymbol{t} \in R^{3\times 1} \qquad \boldsymbol{A} \in R^{3\times 3} \tag{1}$$

where $\boldsymbol{A}$ defines an arbitrary rotation and scaling and $\boldsymbol{t}$ defines a translation. A more compact representation of a combined rotation and a translation can be obtained when an additional coordinate is introduced:

$$\begin{pmatrix} x_1 \\ x_2 \\ x_3 \\ 1 \end{pmatrix}' = \begin{pmatrix} r_{1,1} & r_{1,2} & r_{1,3} & t_1 \\ r_{2,1} & r_{2,2} & r_{2,3} & t_2 \\ r_{3,1} & r_{3,2} & r_{3,3} & t_3 \\ 0 & 0 & 0 & 1 \end{pmatrix} \begin{pmatrix} x_1 \\ x_2 \\ x_3 \\ 1 \end{pmatrix} \Leftrightarrow \boldsymbol{x}' = \boldsymbol{M} \cdot \boldsymbol{x} \tag{2}$$

Besides the more compact representation the computational power of matrix-oriented packages such as Matlab (The MathWorks, Natick, MA), which is used here for implementation, can be optimally exploited. Unless otherwise noted all points in this contribution are specified in homogeneous coordinates.

The coordinate system of the agglomerate has its origin in the center of mass of the agglomerate. The orientation of this coordinate system will be discussed in the section on the substitution systems. For now, let the orientation be completely arbitrary.

To determine the position of a primary particle within an agglomerate, it is now necessary to define the position and orientation of each primary particle coordinate system within the agglomerate coordinate system. Mathematically, this can be represented by the transformation matrix $\boldsymbol{M}$, which transforms (rotates and translates) the primary particle coordinate system to the agglomerate coordinate system. Thus, each agglomerate is fully defined by a number of primary particles with given side length halves and given transformation matrix. Having defined l_1, l_2, and l_3 as well as the transformation matrix $\boldsymbol{M}$ for each primary particle in an agglomerate, the geometry is completely specified, although geometry is not the only important parameter for agglomerated primary particles. Consider two primary particles being attached to each other. If the particle is subject to surface growth, the faces where the particles are attached to each other will no longer be able to grow. Therefore, each primary particle face will additionally be characterized by a growth flag g_j specifying whether the face is still able to grow (value = 1) or whether the growth of the face is geometrically hindered by attached particles (value = 0):

$$\boldsymbol{g} = (g_1, g_2, g_3, g_4, g_5, g_6)^T \tag{3}$$

For the association of the vector entries to the faces see Figure 1.

The complete characterization of the particle ensemble is therefore given by

$$\boldsymbol{l}^{(i,j)}, \qquad \boldsymbol{g}^{(i,j)}, \qquad \boldsymbol{M}^{(i,j)} \tag{4}$$

where $i = 1, \ldots, n_{\text{agg}}$ specifies the single agglomerates and $j = 1, \ldots, n_{\text{pp},i}$ determines a single primary particle within the agglomerate i. In the following the upper index (i, j) will frequently be used to address primary particles j within an agglomerate i. This may also include single primary particles. In that case the number of primary particles $n_{\text{pp},i}$ in the agglomerate i will be 1.

Altogether, this gives a quite detailed representation of both primary particles and agglomerated structures. However, especially for evaluation of an aggregation event this detailed description is rather complex, making the determination of a newly formed agglomerate resulting from the aggregation of already existing agglomerate structures very tedious. Although in principle a rigorous determination of the contact points of two agglomerates with arbitrary orientation to each other is possible, it must be expected to be very time consuming. To improve performance, it is therefore suggested to introduce another hierarchical level of detail for the agglomerate characterization that can be used for aggregation events without losing too much of the realistic description of the geometry.

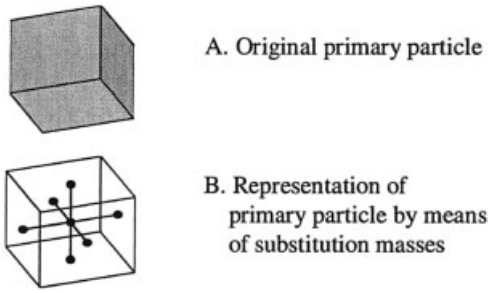

Figure 2. Simple mass point substitution system for primary particle.

Substitution Systems. The low complexity level characterization of agglomerate structures constitutes a system of point masses. This substitute point mass system should preserve as many properties of the original system as possible. Considering only a single nonagglomerated primary particle, a system of seven substituting point masses is introduced. One point mass is positioned in the center of mass, whereas two mass points are positioned at opposite sides of each coordinate axis (see Figure 2). The position and the actual value for the substitution masses can uniquely be defined by demanding the preservation of the center of mass, the preservation of the moment of inertia with respect to the coordinate axes, and considering the overall extension of the primary particle. These restrictions result in the trivial solution of six point masses, which are located in the centers of the faces of the primary particle. Each of these point masses is just one sixth of the total mass of the primary particle $m_{\text{pp}}^{(i,j)}$. The mass point in the center of the particle has the value 0. Thus only six point masses are actually necessary. The formulation of the restrictions and the derivation of the resulting system are given in the Appendix. According to that derivation the substitution system can be represented by

$$\boldsymbol{X}_{\text{pp,subst}}^{(i,j)} = [\boldsymbol{x}_1^{(i,j)}, \ldots, \boldsymbol{x}_6^{(i,j)}] = \begin{bmatrix} l_1^{(i,j)} & 0 & 0 & -l_1^{(i,j)} & 0 & 0 \\ 0 & l_2^{(i,j)} & 0 & 0 & -l_2^{(i,j)} & 0 \\ 0 & 0 & l_3^{(i,j)} & 0 & 0 & -l_3^{(i,j)} \\ 1 & 1 & 1 & 1 & 1 & 1 \end{bmatrix} \tag{5}$$

$$\boldsymbol{m}_{\text{pp,subst}}^{(i,j)} = \frac{m_{\text{pp}}^{(i,j)}}{6}(1, 1, 1, 1, 1, 1) \tag{6}$$

The substitution system for an agglomerate structure is less obvious. For consistency, the substitution system of the agglomerate structure should be of the same character as the primary particle substitution system. Thus, a coordinate system should be constructed such that seven point masses reflect the main geometry and behavior of the agglomerate.

The determination of the substitution systems is based on all the substitute masses of the primary particles (see Figure 3B). These constitute a set of mass points in an arbitrary agglomerate coordinate system:

$$\boldsymbol{X}_{\text{agg}}^{(i)} = [\boldsymbol{M}^{(i,1)} \cdot \boldsymbol{X}_{\text{pp,subst}}^{(i,1)}, \ldots, \boldsymbol{M}^{(i,n_{\text{pp},i})} \cdot \boldsymbol{X}_{\text{pp,subst}}^{(i,n_{\text{pp},i})}] \tag{7}$$

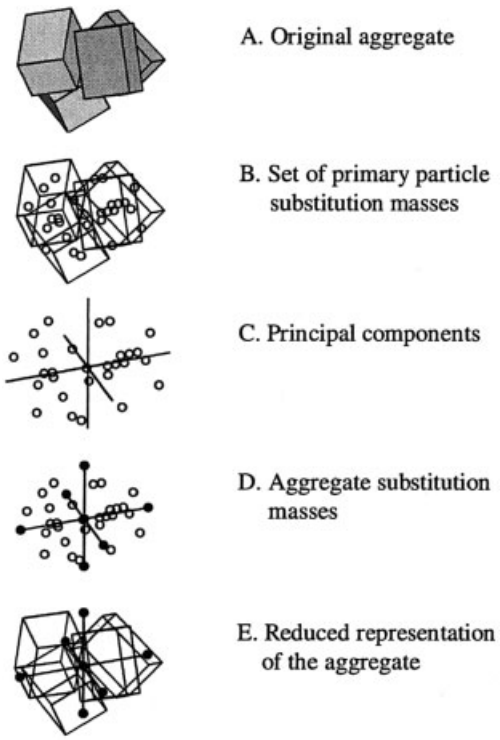

Figure 3. Construction of the mass point substitution system from the point masses substituting the primary particles.

$$\boldsymbol{m}_{\mathrm{agg}}^{(i)} = [\boldsymbol{m}_{\mathrm{pp,subst}}^{(i,1)}, \ldots, \boldsymbol{m}_{\mathrm{pp,subst}}^{(i,n_{\mathrm{pp},i})}] \tag{8}$$

Recall that the matrices $\boldsymbol{M}^{(i,j)}$ reflect the transformation of the coordinates system of primary particle j to the coordinate system of the agglomerate i. Without restriction of generality, we can assume that the origin of the agglomerate coordinate system is in the center of mass of the set of mass points $\boldsymbol{X}_{\mathrm{agg}}^{(i)}$. Unless this was true a simple translational operation that would just give different values of $\boldsymbol{M}^{(i,j)}$ would ensure this assumption. Note that the center of mass of the set of mass points $\boldsymbol{X}_{\mathrm{agg}}^{(i)}$ by definition also is the center of mass of the real set of primary particles.

The seven point masses should again be positioned on the axes of the agglomerate coordinate system. Until now the coordinate system of the agglomerate was arbitrarily oriented.

To reflect the overall geometry of the agglomerate a principal components analysis (PCA) is performed. The resulting principal components are used as the axes of the agglomerate coordinate system (see Figure 3C). To account for the different masses of the mass points the positions are weighted by the corresponding mass*:

$$[\boldsymbol{D}^{(i)} \quad \tilde{\boldsymbol{m}}^{i}] = [\boldsymbol{m}_{\mathrm{pp,subst}}^{(i,1)}\boldsymbol{M}^{(i,1)} \cdot \boldsymbol{X}_{\mathrm{pp,subst}}^{(i,1)}, \ldots, \boldsymbol{m}_{\mathrm{pp,subst}}^{(i,n_{\mathrm{pp},i})}\boldsymbol{M}^{(i,n_{\mathrm{pp},i})} \cdot \boldsymbol{X}_{\mathrm{pp,subst}}^{(i,n_{\mathrm{pp},i})}]^{T} \tag{9}$$

Note that the data matrix $\boldsymbol{D}^{(i)}$ constitutes only Cartesian coordinates because no translation will be involved in determining the new directions. A PCA of $\boldsymbol{D}^{(i)}$ will therefore yield the directions of the maximum variance of the mass distribution in the agglomerate. Given that the mass-weighted matrix is centered—recall that the current coordinate system has its origin at the center of mass—a singular value decomposition

$$\boldsymbol{D}^{(i)} = \boldsymbol{U}^{(i)}\boldsymbol{S}^{(i)}[\boldsymbol{V}^{(i)}]^{T} \tag{10}$$

yields the desired principal components. The principal components of the mass weighted matrix $\boldsymbol{D}^{(i)}$ are just the columns of the 3×3 matrix $\boldsymbol{V}^{(i)}$.[39] These principal components are now used as the axes of the new coordinate system:

$$\boldsymbol{I}\boldsymbol{X}_{\mathrm{agg}}^{(i)} = \begin{bmatrix} \boldsymbol{V}^{(i)} & \boldsymbol{0} \\ \boldsymbol{0} & 1 \end{bmatrix}[\boldsymbol{X}_{\mathrm{agg}}^{(i)}]' \Rightarrow \tag{11}$$

$$[\boldsymbol{X}_{\mathrm{agg}}^{(i)}]' = \begin{bmatrix} [\boldsymbol{V}^{(i)}]^{-1} & \boldsymbol{0} \\ \boldsymbol{0} & 1 \end{bmatrix}\boldsymbol{X}_{\mathrm{agg}}^{(i)} \tag{12}$$

The rows of the matrix $[\boldsymbol{X}_{\mathrm{agg}}^{(i)}]'$ now hold the positions of the primary particle substitution masses in the system of the principal components in homogeneous coordinates.

Now that the new coordinate system is available, the open question is where to position and which value to assign the seven substitution masses for the agglomerate. The position of the substitution masses should be chosen to reflect the overall geometry of the agglomerate. Here, the maximum $[L_1^{(i)}, L_2^{(i)}, L_3^{(i)}]$ and the minimum $[L_4^{(i)}, L_5^{(i)}, L_6^{(i)}]$ position of all coordinate value of the corners of the primary particles in agglomerate i are chosen. Alternatively, one may chose the maximum and minimum values of the substitution masses of the primary particles. However, this choice implies the possibility that the substitution mass in the origin of the coordinate system becomes negative. Computationally, this is not a problem but somehow contradicts common perception. On the other hand, the choice made here leads to structures where the primary particles may not actually touch each other when the number of primary particles in an agglomerate increases.

To uniquely define the actual value of these seven point masses a set of constraints is imposed. Again the center of mass as well as the moment of inertia with respect to the principal component axes is to be preserved. Again, a derivation of the corresponding result (see Figure 3D) is given in the Appendix.

Consequently, the complete agglomerate is represented by a seven mass point characterization reflecting the overall geometry as well as the micromechanical behavior in a flow field (see also Figure 3E):

$$\boldsymbol{X}_{\mathrm{agg,subst}}^{(i)} = \begin{bmatrix} L_1^{(i)} & 0 & 0 & L_4^{(i)} & 0 & 0 & 0 \\ 0 & L_2^{(i)} & 0 & 0 & L_5^{(i)} & 0 & 0 \\ 0 & 0 & L_3^{(i)} & 0 & 0 & L_6^{(i)} & 0 \\ 1 & 1 & 1 & 1 & 1 & 1 & 1 \end{bmatrix} \tag{13}$$

$$\boldsymbol{m}_{\mathrm{agg,subst}}^{(i)} = (m_{\mathrm{agg,subst},1}^{(i)}, \ldots, m_{\mathrm{agg,subst},7}^{(i)}) \tag{14}$$

The following section will show how the reduced substitution systems for primary particles and agglomerates can be used for formulating crystal growth and aggregation events within a Monte Carlo simulation.

* All the positions at which the corresponding mass is zero are neglected.

Monte Carlo scheme

In contrast to a Lagrangian multiphase simulation, the Monte Carlo scheme used herein does not track the position of the agglomerates in space. Thus, collisions with possible aggregation are not determined a priori but are considered to occur at a given frequency. Generally, one must distinguish between event-based rate processes (nucleation, breakage, aggregation) and continuous rate processes (feed, removal, growth). Only crystal growth and aggregation are considered herein. No new particle formation by any mechanism (primary or secondary nucleation) is used. The aggregation rate β is chosen to be proportional to the square of the number concentration of the particles:

$$\beta = \beta_0 \left(\frac{n_{\text{agg}}}{V_{\text{MC}}} \right)^2 \tag{15}$$

where β_0 is the aggregation rate constant and V_{MC} is the control volume for the Monte Carlo simulation.

The growth rates are assumed to be constant. However, the growth rates G_1, G_2, and G_3 for the three different types of faces may differ from each other.

The algorithm used here is event-driven. Thus, the time between two aggregation events is given by

$$\Delta t = \frac{1}{\beta} \tag{16}$$

After each time step two particles (agglomerates or primary particles) are arbitrarily selected and aggregated according to the procedure given in the following section. After an aggregation event all particles are grown according to the procedure given below.

To compensate the decrease of particle number resulting from aggregation, the procedure by Maisels et al.[31] is followed by adapting the control volume over time. If the number of particles has dropped by 50%, the control volume is doubled. Accordingly, the set of particles is doubled.

Realization of the rate processes

Growth. For nonagglomerated primary particles the growth step is rather trivial. The halved side lengths l_k are just incremented according to the face specific growth rates:

$$l_k^{(i,j)} := l_k^{(i,j)} + G_k \Delta t, \qquad k = 1, 2, 3 \tag{17}$$

In the case of an agglomerate, not all the faces are allowed to grow. According to the growth flag specifications $\boldsymbol{g}^{(i,j)}$ introduced above, only those faces are grown that are "at the outer side" of the agglomerate:

$$l_k^{(i,j)} := l_k^{(i,j)} + \frac{g_k^{(i,j)} + g_{k+3}^{(i,j)}}{2} G_k \Delta t, \qquad k = 1, 2, 3 \tag{18}$$

If the center of mass moves according to nonsymmetric growth, the coordinate system will be translated to remain in the center of mass.

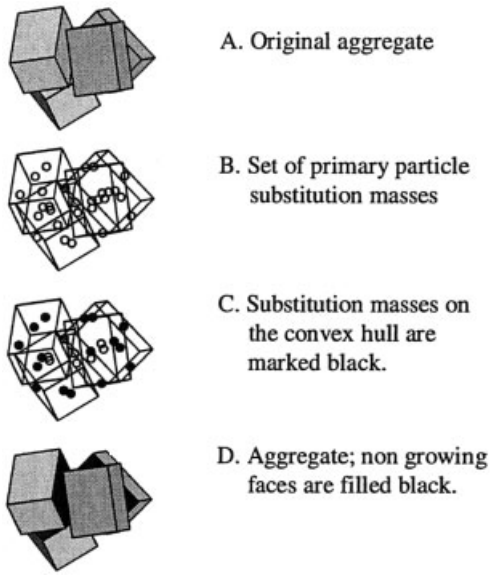

Figure 4. Identification of the growing faces by means of a convex hull operation.

The major question remaining is: How does one identify the growing and nongrowing faces? Again, concepts from computer graphics/computational geometry are used. By a convex hull operation all points of a data set can be identified that construct a minimum convex hull containing all data points. There are numerous algorithms that can be used to determine a convex hull. Here, the standard algorithm given in Matlab[40] is used. Applying a convex hull operation on the set of locations of the primary particle substitution masses identifies the mass points that are "at the outer boundary" of the agglomerate (see Figure 4). Because all primary particle substitution masses are directly associated with the faces of the primary particles, the faces corresponding to the set of point masses of the convex hull are identified as growing faces. All other faces, for which the corresponding mass point lies within the convex hull, are considered to be nongrowing (see Figure 4D).

Aggregation. For aggregation the agglomerate characterization using the seven substitution masses is of major importance. Based on the information content of this characterization many realizations of aggregation events are conceivable. Because the focus of this contribution is on the framework of characterizing the particles, only a simple realization is proposed. First, two particles, which may be agglomerates or single primary particles, are arbitrarily picked from the set of active particles (see Figures 5A and 5B). From each of these agglomerates one of the substitution mass points is arbitrarily selected (see Figure 5C). The particles are reoriented such that the picked mass points coincide and that the corresponding axes are parallel to each other. To allow more flexibility in the formation of aggregates one of the particles is allowed to rotate with an arbitrarily selected angle with respect to the common axis.

Note that in the current realization the aggregations of any agglomerate pairs have the same probability, which may be unrealistic because smaller particles may be more mobile or larger particles have a higher kinetic energy when colliding.

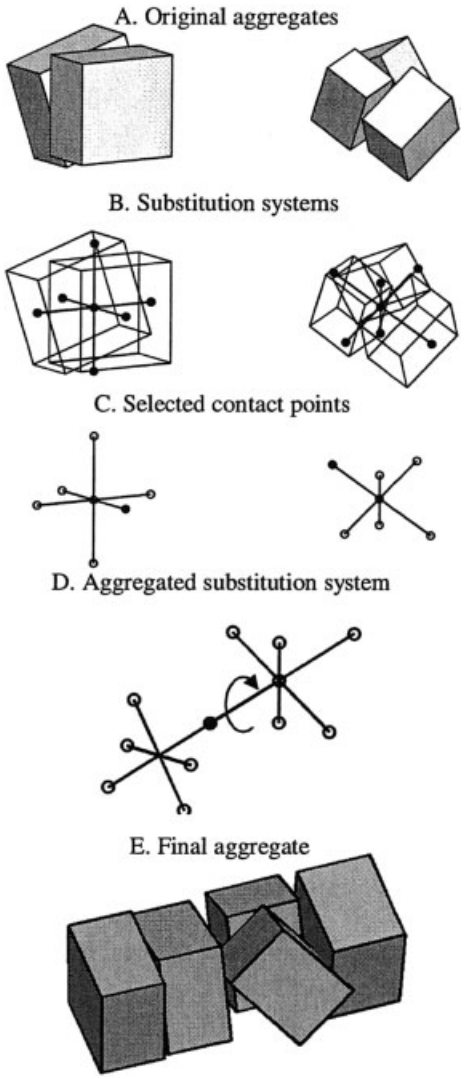

Figure 5. Steps in the realization of an aggregation event.

Simulation Results

To study the behavior of the Monte Carlo model six different cases have been simulated. To model the growth behavior of the primary particles three different scenarios are considered: cubic growth, plate growth, and needle growth using the same growth rate for all three types of faces of the primary particles, two fast/one slow growing faces and one fast/two slow growing faces, respectively. Each of these growth modes has been combined with a high and a low aggregation rate. The values of the used parameters and the initial conditions can be found in Table 1.

As a consistency check, Figure 6 shows the number concentration as a function of time. Because the growth behavior of the particles does not affect the number concentration, only a distinction between the high and the low aggregation rate is necessary. Trivially, the number concentration decreases with time because of the formation of aggregates. In accordance to the notation used in deterministic population balance modeling, the number concentration is denoted by μ_0, which is frequently used for the first-order moment of the particle size distribution. As expected, the number concentration decreases according to the following analytical solution:

$$\mu_0(t) = \frac{\mu_0(t=0)}{1 + \mu_0(t=0)\beta_0 t} \tag{19}$$

Table 1. Parameters for the Monte Carlo Simulations

Initial number of particles [no aggregates, only primary particles ($n_{\mathrm{pp},i} = 1$)]	$n_{\mathrm{agg}}\ (t = 0) = 10^4$
Initial primary particle size	$\boldsymbol{l}^{(i,j)} = (\frac{1}{2}, \frac{1}{2}, \frac{1}{2})^T \cdot 1\ \mu\mathrm{m}$
Initial number concentration	$\mu_0\ (t = 0) = 10^9\ (\mathrm{m}^{-3})$
Cubic growth	$G_1 = 10^{-7}$ (m/s)
	$G_2 = 10^{-7}$ (m/s)
	$G_3 = 10^{-7}$ (m/s)
Plate growth	$G_1 = 10^{-8}$ (m/s)
	$G_2 = 10^{-7}$ (m/s)
	$G_3 = 10^{-7}$ (m/s)
Needle growth	$G_1 = 10^{-8}$ (m/s)
	$G_2 = 10^{-8}$ (m/s)
	$G_3 = 10^{-7}$ (m/s)
Aggregation rate constant (high)	$\beta_0 = 5 \times 10^{-13}\ (\mathrm{m}^3/\mathrm{s})$
Aggregation rate constant (low)	$\beta_0 = 1 \times 10^{-13}\ (\mathrm{m}^3/\mathrm{s})$

To assess the growth behavior, Figure 7 shows the solids volume fraction. As expected, the solids fraction increases more rapidly if all primary particle faces are allowed to grow according to the fast growth rate specification. Therefore, the increase is less pronounced from cubic growth by way of plate growth to needle growth. However, the increase of the solids volume fraction is also affected by the aggregation rate. For a higher aggregation rate, the agglomerate structures become more complex. This leads to shielding effects of some faces. For highly agglomerated particles, not all faces are allowed to grow. Consequently, a higher aggregation rate yields a lower increase in the solids volume fraction.

To quantify this shielding effect, Figure 8 shows the mean fraction of the surface area available for growth and the surface area that would be available for nonagglomerated primary particles:

$$\gamma = \frac{1}{n_{\mathrm{agg}}} \sum_{i=1}^{n_{\mathrm{agg}}} \frac{A^{(i),\mathrm{available\ for\ growth}}}{A^{(i),\mathrm{total}}}, \tag{20}$$

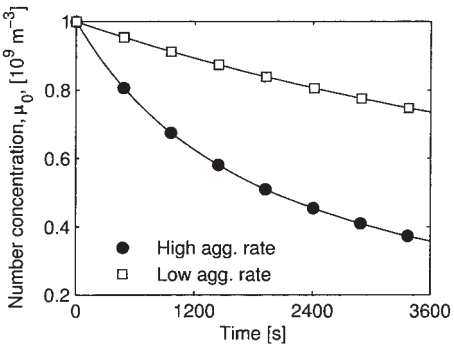

Figure 6. Time evolution of the number concentration for high (filled symbols) and low (open symbols) aggregation rate.

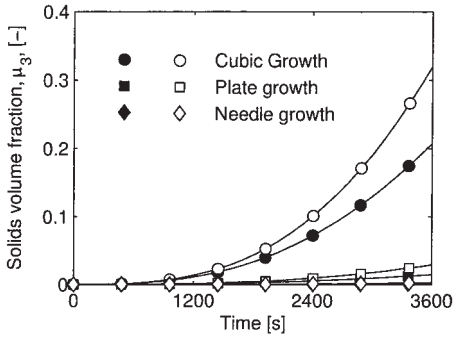

Figure 7. Time evolution of the solids volume fraction for high (filled symbols) and low (open symbols) aggregation rate.

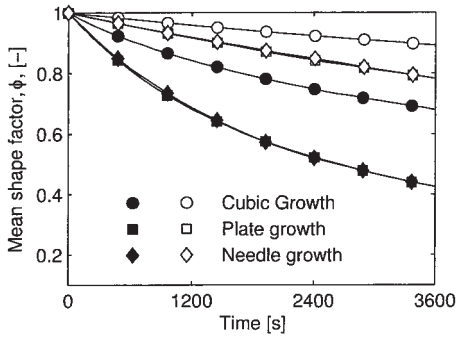

Figure 9. Time evolution of the mean shape factor φ for high (filled symbols) and low (open symbols) aggregation rate.

with

$$\frac{A^{(i),\text{available for growth}}}{A^{(i),\text{total}}} = \left\langle \frac{\sum_{j=1}^{n_{\text{pp},i}} \{[g_1^{(i,j)} + g_4^{(i,j)}] l_2^{(i,j)} l_3^{(i,j)} + [g_2^{(i,j)} + g_5^{(i,j)}] l_1^{(i,j)} l_3^{(i,j)} + [g_3^{(i,j)} + g_6^{(i,j)}] l_1^{(i,j)} l_2^{(i,j)}\}}{2 \sum_{j=1}^{n_{\text{pp},i}} [l_2^{(i,j)} l_3^{(i,j)} + l_1^{(i,j)} l_3^{(i,j)} + l_1^{(i,j)} l_2^{(i,j)}]} \right\rangle \tag{21}$$

The plots show that for lower aggregation the surface area available for growth decreases slower than for the highly aggregating systems. For cubic growth the decrease is less pronounced than for either plate growth or needle growth. In particular, for plate growth the surface area available for growth decreases by about 50%. Perhaps this is an unrealistic value, which must be attributed to the simplifications made for the growth face identification. For agglomerates with a large number of primary plate or needle-shaped particles, only very few points constitute the convex hull of the system, whereas some of the nonidentified faces are actually still exposed to the fluid.

This behavior is also reflected when looking at the evolution of a volumetric shape factor. Because of the high irregularity of the particles, a shape factor that uses the hierarchical characterization is used. The shape factor ϕ here is defined as the fraction of the actual volume of the agglomerate and the volume of the agglomerate substitution system considering a cuboid shape:

$$\phi = \frac{1}{n_{\text{agg}}} \sum_{i=1}^{n_{\text{agg}}} \left\{ \frac{8 \sum_{j=1}^{n_{\text{pp},i}} l_1^{(i,j)} \cdot l_2^{(i,j)} \cdot l_3^{(i,j)}}{[L_1^{(i)} + L_4^{(i)}][L_2^{(i)} + L_5^{(i)}][L_3^{(i)} + L_6^{(i)}]} \right\} \tag{22}$$

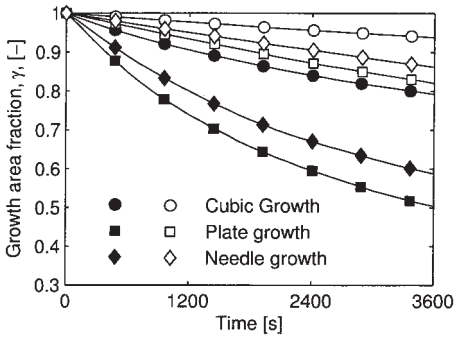

Figure 8. Time evolution of area fraction actually available for growth for high (filled symbols) and low (open symbols) aggregation rate.

For an agglomerate of two equally sized cubic primary particles for which no rotation along the aggregation axis has been performed the shape factor would remain 1, as it is for every primary particle. The shape factor, therefore, characterizes the openness of the agglomerate. Figure 9 shows the evolution of the mean shape factor. The simulations with high aggregation rate all lead to larger agglomerates and, consequently, to more open particle structures. Obviously, the shape factor evolution is the same for both the plate growth and the needle growth in both aggregation cases, whereas cubic growth leads to more compact structures.

An important benefit of the characterization and use of the Monte Carlo approach is that the morphology of the particles can be explicitly accessed. Each and every agglomerate is available in its full three-dimensional shape. Figure 10 shows some particles that are all selected at the end of the simulation time for the different parameter settings. The agglomerate structures show that the produced particles are of a quite realistic shape.

Discussion, Conclusions, and Perspective

The contribution introduces a hierarchical particle characterization that reduces the characterization of the agglomerates by means of substitution systems. By this, the simulation of the evolution of an ensemble of 10,000 particles becomes possible on a state-of-the-art desktop computer (3.06 GHz, 2GB RAM) in a reasonable time (one simulation run took between 4 and 9 h).

According to the construction of the substitution systems, it is possible that two agglomerates form a larger agglomerate without actually touching each other. Although this is physically unreasonable, it is acceptable because this results from the reduction in complexity, which allows the simulation in the

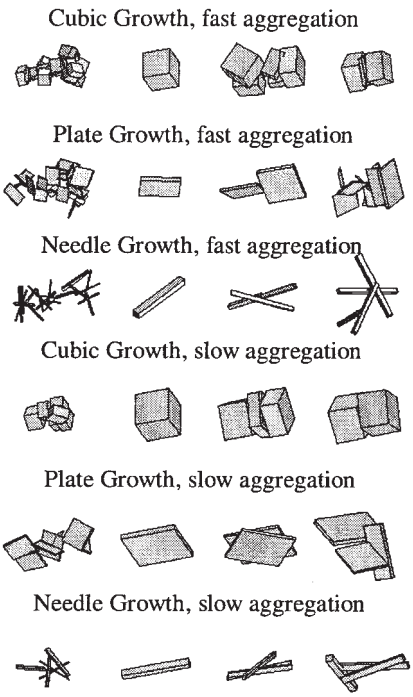

Figure 10. Selected particle morphologies at $t = 3600$ s.

The first and second columns show the particles with the highest degree of agglomeration (that is, the highest number of primary particles per agglomerate) and a particle, which has not yet encountered any aggregation, respectively. The third and fourth columns show arbitrarily selected agglomerates. Note that the scaling for the particles is not identical. Particles should not be compared in size but only with respect to morphology!

first place. Furthermore, this is observed only if the number of primary particles per agglomerate is high (>10).

Another problem observed for highly agglomerated particles is the fact that the identification of the growth faces using the convex hull approach seems to be very restrictive. Very few faces are actually identified as growth faces, whereas visual inspection of the agglomerates suggests making more faces available for growth.

According to these drawbacks, the method seems applicable to systems only where the agglomerates contain a limited number of primary particles (<10). For systems leading to a high degree of agglomeration, extensions to the proposed method may be necessary.

The focus herein has been on the description of the hierarchical particle characterization and its implication. Because of the very simple kinetics, the contribution does not claim to simulate any real physical process. When extending the given case study toward a more realistic system, several extensions may become necessary. Currently, all particles collide with equal and constant probability and instantly stick together. In real systems neither of these assumptions is likely to hold. The collision frequency will be a function of particle size because smaller particles are generally more mobile and on the other side have a smaller cross-sectional area. Additionally, not all particle collisions will result in a successful formation of a new aggregate. The larger the aggregates will become, the stronger are the hydrodynamic forces acting on them, which eventually leads to a disruption of aggregates. To actually account for the local hydrodynamic behavior determining the aggregation rates, an extension to a Lagrangian approach, where the detailed position in the Euclidian space is considered, is conceivable.

Also the scope of problems to be investigated would increase if particle nucleation and a nonstationary supersaturation would be considered. In terms of the characterization, both extensions are straightforward. However, very high nucleation rates may limit the efficiency of the Monte Carlo method because very small time steps will be chosen.

Nevertheless, the generated agglomerate structures appears to be quite realistic, which makes further consideration of the proposed characterization very promising, to address problems, where the shape of the particles is important. However, it is not only from the perspective of product characterization that the proposed hierarchical characterization seems promising. The characterization allows a much more detailed investigation of aggregation, breakage, or growth processes than is possible with a simple one- or even two-dimensional particle characterization in a population balance framework. This can prove valuable for mechanistic modeling of attrition[16,41,42] and aggregation,[43,44] where the geometry of the particles seems to be very important. Additionally, it allows integration of the molecular level knowledge on agglomeration gained from experimental studies.[45,46]

Literature Cited

1. Hulburt HM, Katz S. Some problems in particle technology. *Chem Eng Sci.* 1964;19:555-574.
2. Randolph AD, Larson MA. *Theory of Particulate Processes*. New York, NY: Academic Press; 1971.
3. Kumar S, Ramkrishna D. On the solution of population balance equations by discretization—I. A fixed pivot technique. *Chem Eng Sci.* 1996;51:1311-1332.
4. Kumar S, Ramkrishna D. On the solution of population balance equations by discretization—II. A moving pivot technique. *Chem Eng Sci.* 1996;51:1333-1342.
5. Kumar S, Ramkrishna D. On the solution of population balance equations by discretization—III. Nucleation, growth and aggregation of particles. *Chem Eng Sci.* 1997;52:46591-4679.
6. Braatz RD, Hasebe S. Particle size and shape control in crystallization processes. Proceedings of Chemical Process Control 6, Tucson, AZ; 2001:345-367.
7. Winn D, Doherty MF. Modeling crystal shapes of organic materials grown from solution. *AIChE J.* 2000;46:1348-1367.
8. Bennema P, Meekes H, Boerrigter SXM, Cuppen HM, Deij MA, van Eupen J, Verwer P, Vlieg E. Crystal growth and morphology: New developments in an integrated Hartman–Perdok-connected net-roughening transition theory, supported by computer simulations. *Cryst Growth Des.* 2004;4:989-997.
9. Hill M. Product and process design for structured products. *AIChE J.* 2004;50:1656-1661.
10. Ma DL, Tafti DK, Braatz RD. High-resolution simulation of multidimensional crystal growth. *Ind Eng Chem Res.* 2002;41:6217-6223.
11. Puel F, Fevotte G, Klein JP. Simulation and analysis of industrial crystallization processes through multidimensional population balance equations. Part 1: A resolution algorithm based method of classes. *Chem Eng Sci.* 2003;58:3715-3727.
12. Puel F, Fevotte G, Klein JP. Simulation and analysis of industrial crystallization processes through multidimensional population balance equations. Part 2: A study of semi-batch crystallization. *Chem Eng Sci.* 2003;58:3729-3740.
13. Briesen H. Simulation of crystal size and shape by means of a reduced two-dimensional population balance model. *Chem Eng Sci.* 2006;61:104-112.
14. Zhang Y, Doherty MF. Simultaneous prediction of crystal shape and size for solution crystallization. *AIChE J.* 2004;50:2101-2112.

15. Gadewar SB, Doherty MF. A dynamic model for evolution of crystal shape. *J Cryst Growth.* 2004;267:239-250.
16. Witten TA, Sander LM. Diffusion-limited aggregation, a kinetic critical phenomenon. *Phys Rev Lett.* 1981;47:1400-1403.
17. Schmid HJ, Al-Zaitone B, Artelt C, Peukert W. Evolution of the fractal dimension for simultaneous coagulation and sintering. *Chem Eng Sci.* 2006;61:293-305.
18. Gahn C, Mersmann A. Brittle fracture in crystallization processes. Part A. Attrition and abrasion of brittle solids. *Chem Eng Sci.* 1999;54: 1273-1282.
19. Gerstlauer A, Mitrovi ć A, Motz S, Gilles E-D. A population model for crystallization processes using two independent particle properties. *Chem Eng Sci.* 2001;56:2553-2565.
20. Peborgh Gooch JR, Hounslow MJ. Monte Carlo simulation of size-enlargement mechanisms in crystallization. *AIChE J.* 1996;42:1864-1874.
21. Kruis RE, Maisels A, Fissan H. Direct simulation Monte Carlo method for particle coagulation and aggregation. *AIChE J.* 2000;46:1735-1742.
22. Rosner DE, Yu S. MC simulation of aerosol aggregation and simultaneous spheroidization. *AIChE J.* 2001;47:545-561.
23. Lin Y, Lee K, Matsoukas T. Solution of the population balance equation using constant-number Monte Carlo. *Chem Eng Sci.* 2002; 57:2241-2252.
24. Metropolis N, Ulam S. The Monte Carlo method. *J Am Stat Assoc.* 1949;44:335-341.
25. Spielman LA, Levenspiel O. A Monte Carlo treatment for reacting and coalescing dispersed phase systems. *Chem Eng Sci.* 1965;20:247-254.
26. Sha BH, Ramkrishna D, Borwanker JD. Simulation of particulate systems using the concept of the interval of quiescence. *AIChE J.* 1977;23:897-904.
27. Ramkrishna D. Analysis of population balance—IV. The precise connection between Monte Carlo simulation and population balances. *Chem Eng Sci.* 1981;36:1203-1209.
28. Liffman K. A direct simulation Monte-Carlo method for cluster coagulation. *J Comput Phys.* 1992;100:116-127.
29. Smith M, Matsoukas T. Constant-number Monte Carlo simulation of population balances. *Chem Eng Sci.* 1998;53:1777-1786.
30. Tandon P, Rosner DE. Monte Carlo simulation of particle aggregation and simultaneous restructuring. *J Colloid Interface Sci.* 1999;213:273-286.
31. Maisels A, Kruis FE, Fissan H. Direct simulation Monte Carlo for simultaneous nucleation, coagulation, and surface growth in dispersed systems. *Chem Eng Sci.* 2004;59:2231-2239.
32. Goodson M, Kraft M. An efficient stochastic algorithm for simulating nano-particle dynamics. *J Comput Phys.* 2002;183:210-232.
33. Rosner DE, McGraw R, Tandon P. Multivariate population balances via moment and Monte Carlo simulation methods: An important sol reaction engineering bivariate example and "mixed" moments for the estimation of deposition, scavenging, and optical properties for populations of nonspherical suspended particles. *Ind Eng Chem Res.* 2003;42:2699-2711.
34. Haseltine EL, Patience DB, Rawlings JB. On the stochastic simulation of particulate systems. *Chem Eng Sci.* 2005;60:2627-2641.
35. Bernard-Michel B, Pons MN, Vivier H. Quantification, by image analysis, of effect of operational conditions on size and shape of precipitated barium sulphate. *Chem Eng J.* 2002;87:135-147.
36. Brown DJ, Vickers GT, Collier AP, Reynolds GK. Measurement of the size, shape and orientation of convex bodies. *Chem Eng Sci.* 2005;60: 289-292.
37. Calderon De Anda J, Wang XZ, Roberts KJ. Multi-scale segmentation image analysis for the in-process monitoring of particle shape with batch crystallisers. *Chem Eng Sci.* 2005;60:1053-1065.
38. Riesenfeld RF. Homogeneous coordinates and projective planes in computer graphics. *IEEE Comput Graph Appl.* 1981;1:50-55.
39. Wall ME, Rechtsteiner A, Rocha LM. *A Practical Approach to Microarray Data Analysis. Singular Value Decomposition and Principal Component Analysis*. Dordrecht, The Netherlands: Kluwer Academic; 2003:91-109.
40. Barber CB, Dobkin DP, Huhdanpaa HT. The Quickhull algorithm for convex hulls. *ACM Trans Math Software.* 1996;22:469-483.
41. Gahn C, Mersmann A. Brittle fracture in crystallization processes. Part B. Growth of fragments and scale-up of suspension crystallizers. *Chem Eng Sci.* 1999;54:1283-1292.
42. Briesen H. Improving the predictive capabilities of the attrition model according to Gahn and Mersmann. Proceedings of the 16th International Symposium on Industrial Crystallization, Dresden, Germany; 2005.
43. Hounslow MJ, Mumtaz HS, Collier AP, Barrick JP, Bramley AS. A micro-mechanical model for the rate of aggregation during precipitation from solution. *Chem Eng Sci.* 2001;56:2543-2552.
44. Liew TL, Barrick JP, Hounslow MJ. On the contact geometry of aggregating crystals. Proceedings of the 15th International Symposium on Industrial Crystallization, Sorrento, Italy; 2002.
45. Ålander EM, Uusi-Penttilä MS, Rasmuson ÅC. Agglomeration of paracetamol during crystallization in pure and mixed solvents. *Ind Eng Chem Res.* 2004;43:629-637.
46. Ålander EM, Rasmuson ÅC. Mechanisms of crystal agglomeration of paracetamol in acetone–water mixtures. *Ind Eng Chem Res.* 2005;44: 5788-5794.

Appendix: Substitution System Construction

Primary particles

By formulating appropriate constraints the substitution system of point masses can be constructed. The objective of the constraints is to uniquely define the seven point masses $m_{\text{subst},k}^{(i,j)}$ as well as their positions $l_k^{(i,j)}$ on the respective axis. When the coordinate systems has its origin in the center of mass of the primary particle it is obvious from symmetry considerations that

$$m_{\text{pp,subst},k+3}^{(i,j)} = m_{\text{pp,subst},k}^{(i,j)}, \qquad k = 1, 2, 3 \tag{A1}$$

$$l_{\text{subst},k+3}^{(i,j)} = l_{\text{subst},k}^{(i,j)}, \qquad k = \{1, 2, 3\} \tag{A2}$$

For the substitution system to reflect the overall geometry, the locations of the point masses are chosen to be in the center of the faces:

$$l_{\text{subst},k}^{(i,j)} = l_k^{(i,j)}, \qquad k = \{1, 2, 3\} \tag{A3}$$

Thus, the only remaining unknown variables are the substitution masses $m_{\text{pp,subst},1}^{(i,j)}$, $m_{\text{pp,subst},2}^{(i,j)}$, $m_{\text{pp,subst},3}^{(i,j)}$, and $m_{\text{pp,subst},7}^{(i,j)}$. They are specified demanding a preservation of the moment of inertia.

The moments of inertia $J_k^{(i,j)}$, $k = \{1, 2, 3\}$, of a cuboid with the mass $m_{\text{pp}}^{(i,j)}$ for the rotating around its center of mass with respect to the axes x_k are given by

$$J_k^{(i,j)} = \frac{1}{12} m_{\text{pp}}^{(i,j)} \sum_{h=\{1,2,3\}\setminus\{k\}} [2 \cdot l_h^{(i,j)}]^2, \qquad k = \{1, 2, 3\} \tag{A4}$$

The moment of inertia of the substitution system of point masses $m_{\text{pp,subst},k}^{(i,j)}$ are given by

$$\begin{aligned} J_{\text{subst},k}^{(i,j)} &= 2 \sum_{h=\{1,2,3\}\setminus\{k\}} m_{\text{pp,subst},h}^{(i,j)} [l_{\text{pp,subst},h}^{(i,j)}]^2 \\ &= 2 \sum_{h=\{1,2,3\}\setminus\{k\}} m_{\text{pp,subst},h}^{(i,j)} [l_h^{(i,j)}]^2, \qquad k = \{1, 2, 3\} \end{aligned} \tag{A5}$$

Demanding that $J_k^{(i,j)} = J_{k,\text{subst}}^{(i,j)}$, $k = \{1, 2, 3\}$, leads to a linear system in $m_{\text{pp,subst},k}^{(i,j)}$, $k = 1, 2, 3$

$$\begin{bmatrix} J_1^{(i,j)} \\ J_2^{(i,j)} \\ J_3^{(i,j)} \end{bmatrix} = \begin{Bmatrix} 0 & [l_2^{(i,j)}]^2 & [l_3^{(i,j)}]^2 \\ [l_1^{(i,j)}]^2 & 0 & [l_3^{(i,j)}]^2 \\ [l_1^{(i,j)}]^2 & [l_2^{(i,j)}]^2 & 0 \end{Bmatrix} \begin{bmatrix} m_{\text{agg,subst},1}^{(i)} \\ m_{\text{agg,subst},2}^{(i)} \\ m_{\text{agg,subst},3}^{(i)} \end{bmatrix}, \quad \text{(A6)}$$

which has the solution

$$m_{\text{pp,subst},k}^{(i,j)} = \frac{m_{\text{pp}}^{(i,j)}}{6}, \qquad k = 1, 2, 3 \quad \text{(A7)}$$

From the preservation of the total mass

$$\sum_{k=1}^{7} m_{\text{pp,subst},k}^{(i,j)} = m_{\text{pp}}^{(i,j)}, \qquad k = 1, 2, 3 \quad \text{(A8)}$$

it follows that $m_{\text{pp,subst},7}^{(i,j)} = 0$.

Agglomerate particles

The construction of the substitution system for the agglomerates is along the same line as for the primary particle. However, the symmetry assumptions do not necessarily hold. From the maximum and minimum value of the all primary particle corners the locations specified by $L_k^{(i)}$, $k = \{1, \ldots, 6\}$ of the point masses are already known. For the agglomerate i the remaining unknowns are the values of the seven point masses $m_{\text{agg,subst},k}^{(i)}$, $k = \{1, \ldots, 7\}$. For their determination, the preservation of the center of mass (three equations), the moment of inertia (three equations), and the total mass (one equation) is demanded.

The preservation of the center of mass yields

$$m_{\text{agg,subst},k+3}^{(i)} L_{k+3}^{(i)} = m_{\text{agg,subst},k}^{(i)} L_k^{(i)}, \qquad k = \{1, 2, 3\} \quad \text{(A9)}$$

The moments of inertia of the original agglomerate are calculated assuming that the mass of the primary particles is concentrated in the origin of the respective primary particle coordinate system:

$$J_k^{(i)} = \sum_{i=1}^{n_{\text{agg}}} \sum_{j=1}^{n_{\text{pp},i}} m_{\text{pp}}^{(i,j)} \left\{ \left[\boldsymbol{M}^{(i,j)} \cdot \begin{pmatrix} 0 \\ 0 \\ 0 \\ 1 \end{pmatrix} \right]^T \cdot e_k \right\}^2, \qquad k = \{1, 2, 3\} \quad \text{(A10)}$$

where e_k is the unit vector in the direction of the axis k.

The moments of inertia of the agglomerate substitution system are fully equivalent to Eq. A5. Preservation of the moments of inertia consequently leads to the linear system in $m_{\text{agg,subst},k}^{(i)} L_k^{(i)}$, $k = \{1, 2, 3\}$

$$\begin{bmatrix} J_1^{(i)} \\ J_2^{(i)} \\ J_3^{(i)} \end{bmatrix} = \begin{Bmatrix} 0 & [L_2^{(i)}]^2 & [L_3^{(i)}]^2 \\ [L_1^{(i)}]^2 & 0 & [L_3^{(i)}]^2 \\ [L_1^{(i)}]^2 & [L_2^{(i)}]^2 & 0 \end{Bmatrix} \begin{pmatrix} m_{\text{agg,subst},1}^{(i)} \\ m_{\text{agg,subst},2}^{(i)} \\ m_{\text{agg,subst},3}^{(i)} \end{pmatrix}, \quad \text{(A11)}$$

which allows the computation of $m_{\text{agg,subst},k}^{(i)}$, $k = \{1, 2, 3\}$. Equation A9 then yield the masses $m_{\text{agg,subst},k+3}^{(i)}$. Again the mass closure allows computation of the seventh mass point in the origin of the coordinate system:

$$m_{\text{agg,subst},7}^{(i)} = m_{\text{agg}}^{(i)} - \sum_{k=1}^{6} m_{\text{agg,subst},k}^{(i)} \quad \text{(A12)}$$

Manuscript received Aug. 18, 2005, and revision received Mar. 15, 2006.